

Nonuniform random graphs on the plane: A scaling study

C. T. Martínez-Martínez¹, J. A. Méndez-Bermúdez¹, Francisco A. Rodrigues² and Ernesto Estrada³

¹*Instituto de Física, Benemérita Universidad Autónoma de Puebla, Apartado Postal J-48, Puebla 72570, Mexico*

²*Departamento de Matemática Aplicada e Estatística, Instituto de Ciências Matemáticas e de Computação, Universidade de São Paulo-Campus de São Carlos, Caixa Postal 668, 13560-970 São Carlos, São Paulo, Brazil*

³*Institute for Cross-Disciplinary Physics and Complex Systems (IFISC-CSIC-UIB), Campus Universitat de les Illes Balears, E-07122 Palma de Mallorca, Spain*



(Received 7 September 2021; accepted 27 February 2022; published 15 March 2022)

We consider random geometric graphs on the plane characterized by a nonuniform density of vertices. In particular, we introduce a graph model where n vertices are independently distributed in the unit disk with positions, in polar coordinates (l, θ) , obeying the probability density functions $\rho(l)$ and $\rho(\theta)$. Here we choose $\rho(l)$ as a normal distribution with zero mean and variance $\sigma \in (0, \infty)$ and $\rho(\theta)$ as a uniform distribution in the interval $\theta \in [0, 2\pi)$. Then, two vertices are connected by an edge if their Euclidean distance is less than or equal to the connection radius ℓ . We characterize the topological properties of this random graph model, which depends on the parameter set (n, σ, ℓ) , by the use of the average degree $\langle k \rangle$ and the number of nonisolated vertices V_x , while we approach their spectral properties with two measures on the graph adjacency matrix: the ratio of consecutive eigenvalue spacings r and the Shannon entropy S of eigenvectors. First we propose a heuristic expression for $\langle k(n, \sigma, \ell) \rangle$. Then, we look for the scaling properties of the normalized average measure $\langle \bar{X} \rangle$ (where X stands for V_x , r , and S) over graph ensembles. We demonstrate that the scaling parameter of $\langle \bar{V}_x \rangle = \langle V_x \rangle / n$ is indeed $\langle k \rangle$, with $\langle \bar{V}_x \rangle \approx 1 - \exp(-\langle k \rangle)$. Meanwhile, the scaling parameter of both $\langle \bar{r} \rangle$ and $\langle \bar{S} \rangle$ is proportional to $n^{-\gamma} \langle k \rangle$ with $\gamma \approx 0.16$.

DOI: [10.1103/PhysRevE.105.034304](https://doi.org/10.1103/PhysRevE.105.034304)

I. INTRODUCTION

In many complex systems the entities are embedded in a geometric space such that the connections between them are mainly determined by their spatial separations. When representing these systems we deal with the so-called spatial networks [1], where nodes representing the entities of the system are located in a given space, which may include a geographic space, like in the case of road networks [1]. Nodes can also be located in a three-dimensional space like in certain biological networks where the proximity of cells in a biological tissue determines the structure of the network (see Ref. [2]). A list of related examples includes the networks of patches and corridors in a landscape [3], the networks of galleries in animal nests [4,5], the networks of fractures in rocks [6], and networks of wireless communication devices [7–9], such as mobile phones, wireless computing systems, and wireless sensor networks, among others.

In modeling these systems most of the efforts are a continuation of the pioneering work of Gilbert in 1959 when he proposed the random geometric graph (RGG) model [10]. In a RGG the nodes of the graph are distributed randomly and independently in a unit square and two nodes are connected if they are inside a disk of a given radius [11,12]. This kind of random graph has found multiple applications in areas such as modeling of epidemic spreading in spatial populations, which may include cases such the spreading of worms in a computer network, viruses in a human population, or rumors

in a social network [13–17]. Recent modifications known as random rectangular graphs (RRGs) have been applied in a variety of physical scenarios [18–21].

The Gilbert model and their analogies are very useful in situations where the nodes are uniformly distributed in the graph. This is the case for instance when we want to deploy a series of wireless sensors in a given area. In this case RGG or RRG are very useful modeling techniques to characterize the properties of the network emerging from the sensor deployment [22]. However, in the scenarios mentioned before where the nodes are embedded in a given space not necessarily in a uniform way, the consideration of RGG and/or RRG is not the most appropriate one.

Here we propose an extension of the RGG model to consider different degrees of spatial nonuniformity in the graph. First, we characterize the average topological properties of this random graph model. In particular, we propose heuristic expressions for the average degree and the number of nonisolated vertices. Then, within a random matrix theory approach, we characterize the spectral and eigenvector properties of the adjacency matrix. To this end we perform a scaling study of both the ratio of consecutive eigenvalue spacings and the Shannon entropy of eigenvectors.

II. PRELIMINARIES

Let $G = (V, E)$ be a graph where V is the set of vertices and E the set of edges. A RGG is an undirected graph with

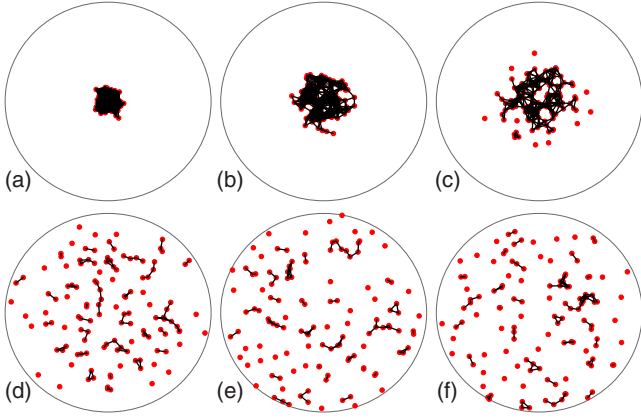


FIG. 1. Examples of RGGs with different degrees of nonuniformity σ : (a) $\sigma = 0.01$, (b) $\sigma = 0.04$, (c) $\sigma = 0.1$, (d) $\sigma = 0.4$, (e) $\sigma = 1$, and (f) $\sigma = \infty$. In all cases we consider $n = 125$ vertices and a connection radius of $\ell = 0.1$.

$n = |V|$ randomly sampled vertices in $[0, 1]^2$, where two vertices are connected by an edge if their Euclidean distance is less than or equal to the parameter ℓ . Here, ℓ is known as the connection radius.

We propose an extension of the RGG model where n vertices are independently distributed in the unit disk with positions, in polar coordinates (l, θ) , obeying the probability density functions $\rho(l)$ and $\rho(\theta)$, respectively. Here we choose $\rho(l)$ as a normal distribution with zero mean and variance σ^2 , $\rho(l) = \mathcal{N}(0, \sigma^2)$, and $\rho(\theta)$ as a uniform distribution in the interval $\theta \in (0, 2\pi)$, $\rho(\theta) = \mathcal{U}(0, 2\pi)$. Indeed, the parameter $\sigma \in (0, \infty)$ accounts for the degree of spatial nonuniformity of the graph; for $\sigma < 1$ a cluster of vertices is formed around the disk center, while for $\sigma \gg 1$ the distribution of vertices becomes uniform within the unit disk. Then, two vertices are connected by an edge if their Euclidean distance is less than or equal to the connection radius $\ell \in [0, 2]$, where 2 corresponds to the diameter of the unit disk, so it is the maximum value that ℓ can take. Therefore, this random graph model depends

on three parameters: the number of vertices, n ; the degree of nonuniformity, σ ; and the connection radius ℓ . Note that both σ and ℓ are given in units of the disk radius, chosen here to be one.

In Fig. 1 we present examples of RGGs with different degrees of nonuniformity, σ , along several orders of magnitude. In all cases we consider $n = 125$ vertices and a connection radius of $\ell = 0.1$. As can be clearly seen from Fig. 1, the random graph model produces a cluster around the disk center for $\sigma < 1$. Formally, it reproduces the RGG model (in the disk) when $\sigma \rightarrow \infty$; however, as can be observed in Fig. 1(d), already for $\sigma = 1$ the vertices appear uniformly distributed. In fact, as will be shown below, $\sigma_c \approx 1$ separates two graph regimes: the *clustering regime* when $\sigma < \sigma_c$ and the *uniform regime* when $\sigma \geq \sigma_c$. We want to add that we choose a disk as the embedding geometry, instead of a square as in other studies of RGGs, to account for the radial symmetry of the vertex distribution.

We characterize the topological properties of our random graph model by the use of the average degree $\langle k \rangle$ and the number of nonisolated vertices V_\times . We note that since the degree distribution $P(k)$ of the graph model proposed here is unimodal and bounded, studying solely its mean is indeed meaningful. We approach their spectral properties with two well-known random matrix theory (RMT) measures on the graph adjacency matrix: the ratio of consecutive eigenvalue spacings r and the Shannon entropy S of eigenvectors.

On the one hand, it is relevant to stress that analytical expressions for both $\langle k \rangle$ and $\langle V_\times \rangle$ on RGGs have been reported recently. In fact, we will make use of those expressions to approach the model of nonuniform RGGs. In particular:

(i) In Ref. [18] the expression for the average degree of RGGs embedded in the unit rectangle was derived; it reads as

$$\langle k \rangle = (n-1)f, \quad (1)$$

where f is a highly nontrivial function of the connection radius ℓ and the rectangle side lengths. Clearly, when the rectangle sides are equal the expression for $\langle k \rangle$ of RGGs embedded in the unit square is obtained; in such a case f gets the form

$$f(\ell) = \begin{cases} \ell^2 \left[\pi - \frac{8}{3}\ell + \frac{1}{2}\ell^2 \right], & 0 \leq \ell \leq 1 \\ \frac{1}{3} - 2\ell^2 \left[1 - \arcsin(1/\ell) + \arccos(1/\ell) \right] + \frac{4}{3}(2\ell^2 + 1)\sqrt{\ell^2 - 1} - \frac{1}{2}\ell^4, & 1 \leq \ell \leq \sqrt{2}. \end{cases} \quad (2)$$

(ii) The average of V_\times can be computed from the average number of isolated vertices $\langle K_1 \rangle$ as $\langle V_\times \rangle = n - \langle K_1 \rangle$. In fact, for standard RGGs, $\langle K_1 \rangle$ is already known [23]; it is given by

$$\langle K_1 \rangle = n(1 - \pi\ell^2)^{n-1} = n \exp(-n\pi\ell^2) - O(n\ell^4).$$

Therefore, for standard RGGs, we can write

$$\langle V_\times \rangle \approx n[1 - \exp(-n\pi\ell^2)]. \quad (3)$$

On the other hand, given the ordered spectra $\{\lambda_i\}$ ($i = 1, \dots, n$) and the corresponding normalized eigenvectors Ψ^i (i.e., $\sum_{j=1}^n |\Psi_j^i|^2 = 1$) of an adjacency matrix, the i th ratio of

consecutive eigenvalue spacings is given by [24]

$$r_i = \frac{\min(\lambda_{i+1} - \lambda_i, \lambda_i - \lambda_{i-1})}{\max(\lambda_{i+1} - \lambda_i, \lambda_i - \lambda_{i-1})}, \quad (4)$$

while the Shannon entropy of the eigenvector Ψ^i reads as

$$S_i = - \sum_{j=1}^n |\Psi_j^i|^2 \ln |\Psi_j^i|^2. \quad (5)$$

We would like to mention that in contrast to the Shannon entropy, which is a well-accepted quantity to measure the degree of disorder in complex networks, the use of the ratio of consecutive eigenvalue spacings is relatively recent in graph studies (see, for example, Refs. [25–28]).

Here, we will follow a recently introduced approach under which the adjacency matrices of random graphs are represented by diluted RMT ensembles; that is, we impose random weights to the adjacency matrix such that we retrieve standard RMT ensembles in the limits of isolated vertices and complete graphs. See the application of this approach on Erdős-Rényi graphs [26,29], RGGs and random rectangular graphs [30], β -skeleton graphs [31], multiplex and multilayer networks [32], and bipartite graphs [27]. Consequently, we define the elements of the adjacency matrix \mathbf{A} of the random graph model as

$$A_{uv} = \begin{cases} \sqrt{2}\epsilon_{uv} & \text{for } u = v \\ \epsilon_{uv} & \text{if there is an edge between vertices } u \text{ and } v \\ 0 & \text{otherwise.} \end{cases} \quad (6)$$

We choose ϵ_{uv} as statistically independent random variables drawn from a normal distribution with zero mean and variance one. Also, $\epsilon_{uv} = \epsilon_{vu}$, since the graphs are assumed as undirected here. Note that the choice of ϵ_{uv} as random numbers with zero mean (i.e., positive and negative numbers) makes the spectra of \mathbf{A} to be centered around zero, which is irrelevant here since we characterize the spectra through eigenvalue spacings [see Eq. (4)]. According to definition (6), diagonal random matrices are obtained for $\ell = 0$ [Poisson ensemble (PE), in RMT terms], whereas the Gaussian orthogonal ensemble (GOE) (i.e., full real and symmetric random matrices) is recovered when $\ell = 2$. Therefore, a transition from the PE to the GOE can be observed by increasing ℓ from zero to two, for any given fixed pair (n, σ) . In fact, this is not the only way to observe the PE-to-GOE transition; it could also be observed by decreasing σ for a given fixed pair (n, ℓ) (see, e.g., Fig. 1) or by increasing n for fixed (σ, ℓ) .

Notice that the random weights we impose to the adjacency matrix in definition (6) do not play any role in the computation of $\langle k \rangle$ or $\langle V_\times \rangle$; however, these weights help us obtaining non-null adjacency matrices (that we can still diagonalize) for graphs with a large number of isolated vertices, so we can safely explore numerically the spectral and eigenvector properties of the model in the limit $\ell \rightarrow 0$.

We want to clarify that the use of RMT ensembles and measures in this study is motivated by the known effectiveness of RMT techniques in problems involving matrices representing complex systems or complex processes (see, e.g., Ref. [33]), including random graphs and networks. We also acknowledge that the weighted adjacency matrices defined in Eq. (6) could be interpreted as a new diluted GOE (recall that there is a diluted GOE that can be understood as based on Erdős-Rényi graphs; see, e.g., Refs. [29,34]). However, it should be noted that the proposed method for building this ensemble is not efficient. In fact, we are not proposing it here as a new RMT ensemble and its main value should be seen in the context of the study of the spectral properties of the random geometric graphs proposed here.

From the definitions above, when $\ell = 0$ (i.e., when all vertices in the graph are isolated) we have $\langle k \rangle_{\text{PE}} = 0$, $\langle V_\times \rangle_{\text{PE}} = 0$, $\langle r \rangle_{\text{PE}} \approx 0.3863$ [24], and $\langle S \rangle_{\text{PE}} = 0$, while when $\ell = 2$ (i.e., when the graph is complete) we have $\langle k \rangle_{\text{GOE}} = n - 1$, $\langle V_\times \rangle_{\text{GOE}} = n$, $\langle r \rangle_{\text{GOE}} \approx 0.5359$ [24], and $\langle S \rangle_{\text{GOE}} \approx$

$\ln(n/2.07)$ [35]. Here and below $\langle \cdot \rangle$ denotes the average over an ensemble of random graphs, in the case of k and V_\times , and the average over all eigenvalues (eigenvectors) of the corresponding adjacency matrices \mathbf{A} in the case of r (S). Specifically, for each combination of parameters (n, σ, ℓ) , we average over ensembles of $10^7/n$ random graph realizations. We want to add that the predictions for $\langle r \rangle_{\text{PE}}$, $\langle r \rangle_{\text{GOE}}$, and $\langle S \rangle_{\text{GOE}}$ reported above are expected for large n ; i.e., finite size effects should be observed for small n , typically for $n < 100$ (see, e.g., Ref. [28]).

III. COMPUTATION OF AVERAGE MEASURES

Now, in Fig. 2 we present $\langle V_\times \rangle$, $\langle r \rangle$, and $\langle S \rangle$ as a function of the connection radius ℓ of nonuniform RGGs of size n (we will consider $\langle k \rangle$ later on). In this figure we are using three values of n : $n = 125$ (left panels), $n = 500$ (middle panels), and $n = 2000$ (right panels). Each panel displays 14 curves corresponding to different degrees of nonuniformity σ (increasing from left to right). In this figure we can clearly see the effect of the parameter σ on the properties of the random graph model: For fixed graph size and fixed connection radius [see, for example, the left vertical dashed line in Fig. 2(a) at $\ell = 0.01$], the graphs may transit from mostly connected (see the left-most curve corresponding to $\sigma = 0.001$) to mostly disconnected (see the right-most curve corresponding to $\sigma = \infty$). This panorama was already shown in Fig. 1; however, in that example the graph does not become disconnected even when $\sigma \rightarrow \infty$ due to the use of a larger value of ℓ : $\ell = 0.1$ [see the right vertical dashed line in Fig. 2(a)].

Indeed, several facts can be highlighted from Fig. 2:

(i) All curves $\langle X \rangle$ vs ℓ in all panels show a smooth transition (in semilogarithmic scale) from the PE to the GOE for increasing ℓ ; the PE and GOE limits are indicated as horizontal dashed lines (lower and upper, respectively). Here and below X stands for V_\times , r , or S .

(ii) For fixed n (σ) the curves $\langle X \rangle$ vs ℓ have a very similar functional form but they are displaced to the right on the ℓ axis for increasing σ (n).

(iii) Thus, the onset of the GOE limit is reached for smaller values of ℓ the larger the values of n and σ are.

(iv) However, once $\sigma \geq \sigma_c$, with $\sigma_c \approx 1$, the curves $\langle X \rangle$ vs ℓ do not change by further increasing σ .

(v) Small-size effects in $\langle r \rangle$ are particularly visible when $\ell \rightarrow 0$ and $\ell \rightarrow 2$ in the case of $n = 125$ [see Fig. 2(d)].

It is relevant to stress that we validated observation (iv) for many other graph sizes, which allowed us to conclude that $\sigma_c \approx 1$ separates two regimes of the random graph model: the *clustering regime* when $\sigma < \sigma_c$ and the *uniform regime* when $\sigma \geq \sigma_c$. In the clustering regime we do observe a cluster of vertices around the disk center [see, e.g., Figs. 1(a)–1(c)], while in the uniform regime the vertices are evenly distributed over the unit disk [see, e.g., Figs. 1(d) and 1(e)].

Moreover, given the similar functional form of the curves $\langle X \rangle$ vs ℓ for different combinations of n and σ , as reported in Fig. 2, it seems that they could be effectively scaled. That is, one should be able to find a scaling parameter $\xi \equiv \xi(n, \sigma, \ell)$

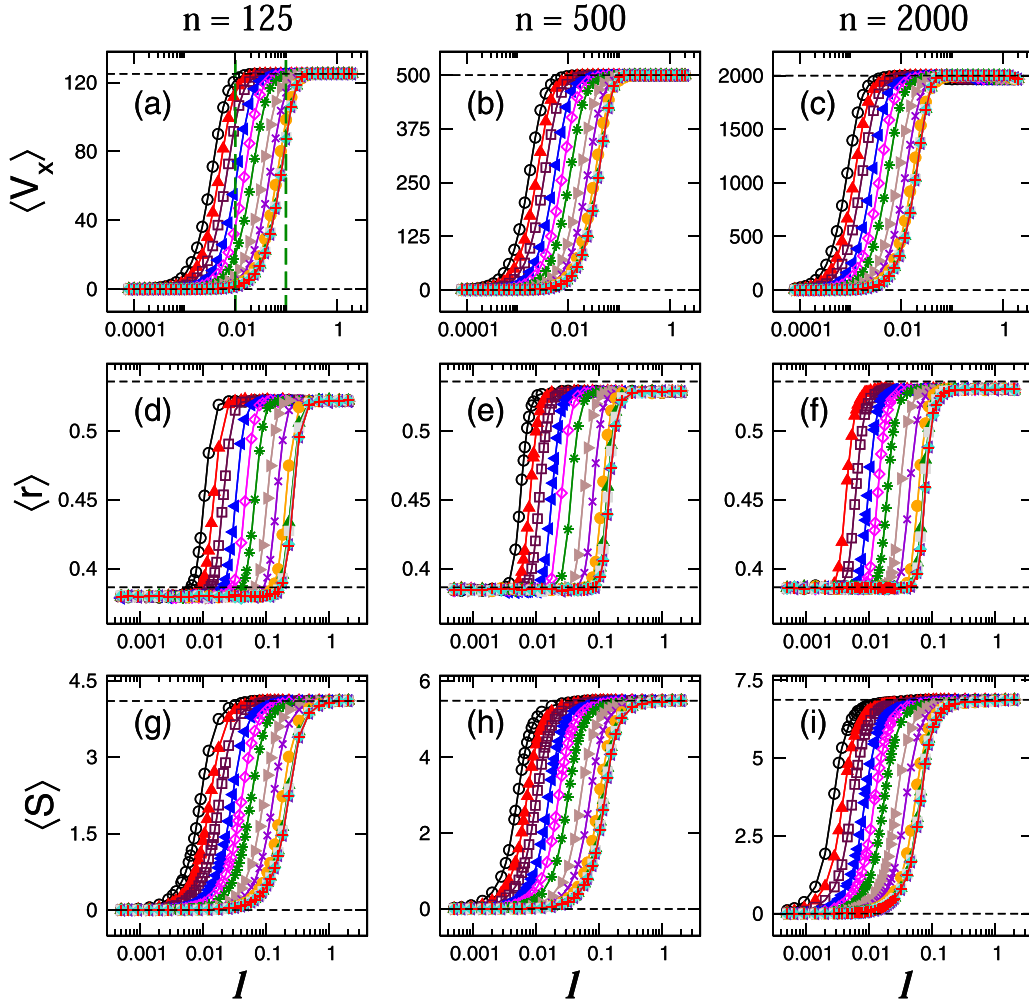


FIG. 2. [(a)–(c)] Average number of nonisolated vertices $\langle V_x \rangle$, [(d)–(f)] average ratio of consecutive eigenvalue spacings $\langle r \rangle$, and [(g)–(i)] average Shannon entropy $\langle S \rangle$ as a function of the connection radius ℓ of nonuniform RGGs of size n : [(a), (d), (g)] $n = 125$, [(b), (e), (h)] $n = 500$, and [(c), (f), (i)] $n = 2000$. Each panel displays 14 curves corresponding to different degrees of nonuniformity σ : $\{0.001, 0.002, 0.004, 0.01, 0.02, 0.04, 0.1, 0.2, 0.4, 0.8, 1, 10, 100, \infty\}$, from left to right. Horizontal dashed lines (lower and upper, respectively) indicate the predictions for the PE and GOE limits. The vertical dashed lines in (a) mark $\ell = 0.01$ and 0.1 ; 0.1 is the value of ℓ used in Fig. 1. Each data value was computed by averaging over $10^7/n$ random graphs.

such that the curves $\langle \bar{X} \rangle$ vs ξ are invariant, where \bar{X} is the properly normalized measure X .

Since in previous studies of RGGs (embedded in the unit square) the average degree $\langle k \rangle$ was shown to play a prominent role in the scaling of topological properties [25,36], before performing the scaling analysis of our random graph model, in the next section we focus on its average degree.

IV. AVERAGE DEGREE

We numerically found that the expression for $\langle k \rangle$ reported in Ref. [18], for the particular case of RGGs embedded in the unit square, works pretty well for our model of nonuniform RGGs in the unit circle by properly choosing an effective connection radius L . That is, we propose the following heuristic expression for $f(L)$:

$$f(L) = \begin{cases} L^2 \left[\pi - \frac{8}{3}L + \frac{1}{2}L^2 \right], & 0 \leq L \leq 1 \\ \frac{1}{3} - 2L^2 \left[1 - \arcsin(1/L) + \arccos(1/L) \right] + \frac{4}{3}(2L^2 + 1)\sqrt{L^2 - 1} - \frac{1}{2}L^4, & 1 \leq L \leq \sqrt{2} \\ 1, & L \geq \sqrt{2}. \end{cases} \quad (7)$$

When setting $L = \ell$, Eqs. (1) and (7) provide the average degree of RGGs embedded in the unit square [see Eq. (2)]. Notice, however, that the last condition in Eq. (7) was included to fit the random graph model proposed here; it does not apply

to RGGs in the unit square since there ℓ cannot be larger than $\sqrt{2}$.

Specifically, Eqs. (1) and (7) provide a good approximation of $\langle k \rangle$ of nonuniform RGGs in the unit circle if $L = \alpha\ell/\sqrt{\pi}$,

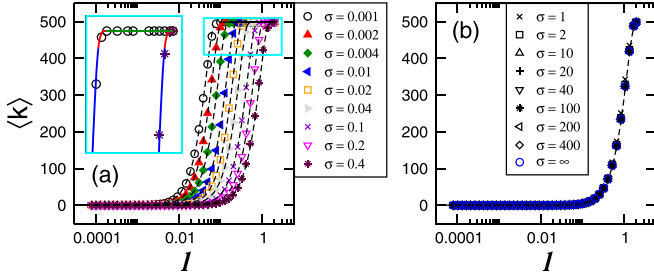


FIG. 3. Average degree $\langle k \rangle$ as a function of the connection radius ℓ of nonuniform RGGs of size $N = 500$ with (a) $\sigma < 1$ and (b) $\sigma \geq 1$. Each data value was computed by averaging over $10^7/n$ random graphs. Dashed lines correspond to Eqs. (1) and (7). The inset in (a) is an enlargement of the cyan rectangle where the data for $\sigma = 0.001$ (circles) and $\sigma = 0.4$ (asterisks) are shown together with Eqs. (1) and (7); there, blue, red, and green lines correspond to the first, second, and third conditions of Eq. (7), respectively.

with $\alpha = \sqrt{2/3\sigma}$ for $\sigma < \sigma_c$ and $\alpha = 1$ for $\sigma \geq \sigma_c$, with $\sigma_c \approx 1$. To verify this claim, in Fig. 3 we plot $\langle k \rangle$ as a function of ℓ of nonuniform RGGs in the unit circle with both $\sigma < \sigma_c$ and $\sigma \geq \sigma_c$; there, the good correspondence between numerical calculations (symbols) and Eqs. (1) and (7) (dashed lines) is evident. Moreover, in the inset of Fig. 3(a) we show the contribution of the three conditions of Eq. (7) to the curves $\langle k \rangle$ vs ℓ of two examples of nonuniform RGGs. In Fig. 3 we consider the fixed graph size $N = 500$ but we observed equivalent plots for any other graph sizes we tested.

We want to recall that $\sigma_c \approx 1$ indeed separates two regimes in the nonuniform RGG model we study here: the clustering regime when $\sigma < \sigma_c$ and the uniform regime when $\sigma \geq \sigma_c$. However, these two regimes will not be evident in the scaling we will perform below since, through the effective connection radius L , both are already incorporated in the definition of $\langle k \rangle$ (that we will use to find the scaling parameters of $\langle V_x \rangle$, $\langle r \rangle$, and $\langle S \rangle$). Moreover, the two regimes can be clearly identified in a *straightforward* scaling analysis, as shown in Sec. V D [see, e.g., Figs. 12(d)–12(f)].

V. SCALING ANALYSIS

A. Average number of nonisolated vertices

Remarkably, taking as a reference Eq. (3), we found that

$$\langle V_x \rangle \approx n[1 - \exp(-n\pi L^2)] \quad (8)$$

approximates well $\langle V_x \rangle$ of nonuniform RGGs in the unit circle if $L = \alpha\ell/\sqrt{\pi}$, with $\alpha = \sqrt{2/3\sigma}$ for $\sigma < \sigma_c$ and $\alpha = 1$ for $\sigma \geq \sigma_c$; this is in line with the proposal of Eq. (7) from Eq. (2). Thus, in Fig. 4 we contrast Eq. (8) with numerical data. There we plot $\langle V_x \rangle$ as a function of ℓ for RGGs in the unit square, in the unit circle as well as for two examples of nonuniform RGGs. In all cases we observe good correspondence between numerical calculations (symbols) and Eq. (8) (dashed lines).

Moreover, it is interesting to notice that from Eqs. (1) and (7), when $L \ll 1$, we can write $\langle k \rangle \approx n\pi L^2$ which coincides with the argument of the exponential in Eq. (8). This allows us to relate $\langle V_x \rangle$ and $\langle k \rangle$ as

$$\langle V_x \rangle \approx n[1 - \exp(-\langle k \rangle)]. \quad (9)$$

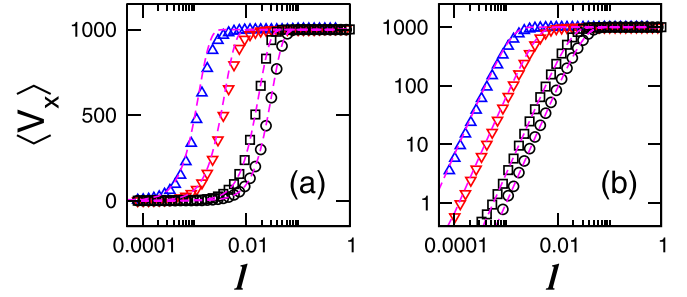


FIG. 4. (a) Average number of nonisolated vertices $\langle V_x \rangle$ as a function of the connection radius ℓ for RGGs embedded in the unit circle (circles), RGGs embedded in the unit square (squares), and nonuniform RGGs with $\sigma = 0.01$ (inverted triangles) and $\sigma = 0.001$ (triangles), from right to left. In all cases $n = 1000$ was used. Dashed lines correspond to Eq. (8). (b) Same as in (a) but in log-log scale to better observe the region $\ell \ll 1$.

Equation (9) implies that the scaling parameter, $\xi \equiv \xi(n, \sigma, \ell)$, of $\langle \bar{V}_x \rangle = \langle V_x \rangle/n$ of nonuniform RGGs is in fact $\langle k \rangle$; that is, if we plot $\langle \bar{V}_x \rangle$ as a function of $\langle k \rangle$, curves corresponding to different parameter combinations (n, σ, ℓ) will fall on top of the universal curve given by Eq. (9). Indeed, in Fig. 5 we present the curves of $\langle \bar{V}_x \rangle$ (divided by n) of Figs. 2(a)–2(c) but now as a function of $\langle k \rangle$ and observe, as expected, that all curves $\langle \bar{V}_x \rangle$ vs $\langle k \rangle$ fall one on top of the other [except for small differences in the interval $1 < \langle k \rangle < 10$ (see the insets); these differences are observed when $\sigma < 1$]. In all panels we also plot Eq. (9) as dashed lines and observe a very good correspondence with the numerical data, which is quite remarkable since Eq. (9) was expected to work only in the limit of $L \ll 1$.

The scaling of $\langle V_x \rangle/n$ of nonuniform RGGs with the average degree, see Fig. 5, agrees with the scaling of several (normalized) topological indices with $\langle k \rangle$ as reported in Refs. [25,36] for Erdős-Rényi graphs and RGGs in the unit square. However, here we are providing an explicit expression for the scaling [see Eq. (9)]. Moreover, we expect other topological indices on nonuniform RGGs to be also scale invariant with $\langle k \rangle$ (see the next section, where it is shown that the Randić connectivity index also scales with $\langle k \rangle$).

B. Randić connectivity index

As already mentioned in the previous section, the scaling of $\langle V_x \rangle/n$ of nonuniform RGGs with the average degree, see Fig. 5, makes us expect other topological indices on nonuniform RGGs to be also scale invariant with $\langle k \rangle$. Thus, in the following we verify this expectation by the use of the Randić connectivity index R .

The *Randić connectivity index* was defined in Ref. [37] as

$$R = \sum_{uv} \frac{1}{\sqrt{d_u d_v}}, \quad (10)$$

where uv denotes the edge of the graph connecting the vertices u and v , and d_u is the degree of the vertex u . In addition to the multiple applications of the Randić index in physical chemistry, being one of the most popular topological indices (see, e.g., Refs. [38–40] and the references therein), this index

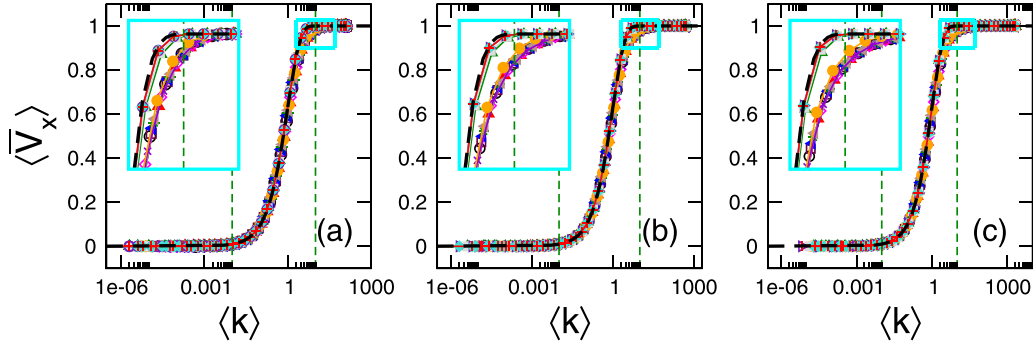


FIG. 5. Average number of nonisolated vertices $\langle V_x \rangle$, normalized to n , as a function of the average degree $\langle k \rangle$ of nonuniform RGGs. (a) $n = 125$, (b) $n = 500$, and (c) $n = 2000$. Each panel displays the 14 curves reported in Figs. 2(a)–2(c). The insets are enlargements of the cyan rectangles of the main panels. Dashed lines correspond to Eq. (9). Vertical dashed lines at $\langle k \rangle = 0.01$ and 10 mark, approximately, the onset of delocalization and the onset of the GOE regime, respectively.

has found several applications in other research areas and topics, such as information theory [41], network similarity [42], protein alignment [43], network heterogeneity [44], and network robustness [45]. However, its use in the study of random graphs has been scarce. For recent exceptions see Refs. [25,36,46], where the average Randić index has been used to probe the percolation transition in Erdős-Rényi graphs and RGGs.

In Fig. 6 we present the normalized average Randić index $\langle \bar{R} \rangle$ as a function of the average degree $\langle k \rangle$ of nonuniform RGGs of size n . As for $\langle V_x \rangle$, we normalize $\langle R \rangle$ to the maximum value it can take: $\langle \bar{R} \rangle \equiv \langle R \rangle / \langle R \rangle_{\text{GOE}}$, with $\langle R \rangle_{\text{GOE}} = n/2$. As anticipated, we observe that $\langle \bar{R} \rangle$ is properly scaled with $\langle k \rangle$, except for the region of large $\langle k \rangle$ (see the insets) where we observe two sets of curves falling one on top of the other: one set corresponding to $\sigma < 1$ and the other to $\sigma \geq 1$. This effect is equivalent to that observed for $\langle V_x \rangle$ (see the insets of Fig. 5).

At this point it is relevant to recall that in Ref. [25] it was shown that $\langle V_x \rangle$ and $\langle R \rangle$ on RGGs are highly correlated, which also occurs for nonuniform RGGs, as can be clearly seen in Figs. 7(a) and 7(b) where we plot $\langle V_x \rangle$ vs $\langle R \rangle$ for nonuniform RGGs with $\sigma < 1$. Moreover, Fig. 7 also suggests that

$$\langle V_x \rangle \approx 2\langle R \rangle \quad (11)$$

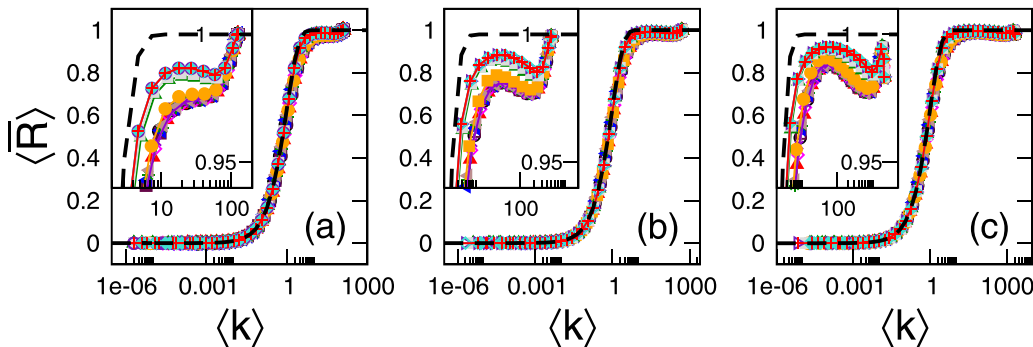


FIG. 6. Average Randić index $\langle R \rangle$ normalized to $n/2$ for (a) $n = 125$, (b) $n = 500$, and (c) $n = 2000$ as a function of the average degree $\langle k \rangle$ of nonuniform RGGs. Each panel displays 14 curves corresponding to different degrees of nonuniformity σ : $\{0.001, 0.002, 0.004, 0.01, 0.02, 0.04, 0.1, 0.2, 0.4, 0.8, 1, 10, 100, \infty\}$. Dashed line in all panels is Eq. (12). Each data value was computed by averaging over $10^7/n$ random graphs.

(see the dashed lines on top of the data in Fig. 7). Thus, Eq. (11) in addition to Eq. (9) allows us to propose

$$\langle R \rangle \approx (n/2)[1 - \exp(-\langle k \rangle)], \quad (12)$$

which in fact coincides relatively well with the numerical data reported in Fig. 6 (see the dashed lines), except for the region of large $\langle k \rangle$ where significant differences between Eq. (12) and the numerical data are evident (see the insets).

It is fair to admit that the log-log scale we used to present the data in Fig. 7 makes the approximation of Eq. (11) look very accurate, but it is not. Then, to quantify the accuracy of Eq. (11) we will make use of the heterogeneity index [44]

$$h = \sum_{uv} \left(\frac{1}{\sqrt{d_u}} - \frac{1}{\sqrt{d_v}} \right)^2, \quad (13)$$

which can be written in terms of V_x and R as

$$h = \sum_{uv} \left(\frac{1}{d_u} + \frac{1}{d_v} \right) - 2 \sum_{uv} \left(\frac{1}{\sqrt{d_u d_v}} \right) = V_x - 2R. \quad (14)$$

Note that Eq. (11) implies $\langle h \rangle \approx 0$ for any combination of parameters (n, σ, ℓ) . Nevertheless, as clearly shown in Fig. 8 (where we plot $\langle h \rangle/n$ vs $\langle k \rangle$ for nonuniform RGGs of different sizes and nonuniformity strengths σ), the curves $\langle h \rangle$ vs $\langle k \rangle$ develop a two-peak structure for $\langle k \rangle \gtrsim 1$ with maxima

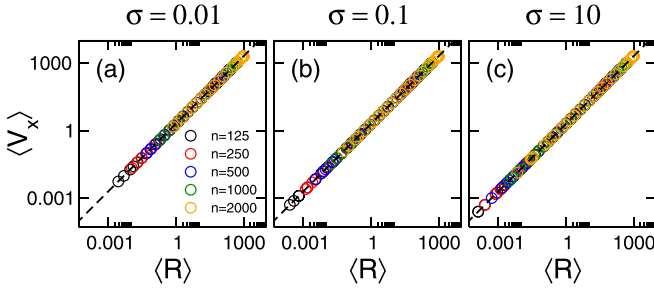


FIG. 7. Average number of nonisolated vertices $\langle V_x \rangle$ as a function of the average Randić index $\langle R \rangle$ of nonuniform RGGs of several sizes n characterized by (a) $\sigma = 0.01$, (b) $\sigma = 0.1$, and (c) $\sigma = 10$. The dashed line on top of the data is $\langle V_x \rangle = 2\langle R \rangle$. Each data value was computed by averaging over $10^7/n$ random graphs.

closer to 0.03. This means that the approximate expression of Eq. (11) has a maximal error of 3%. Also note that the two-peak structure changes with n , differently for $\sigma < 1$ and $\sigma \geq 1$, making $\langle \bar{h} \rangle$ nonscalable. We also found that for large enough n the curves $\langle \bar{h} \rangle$ vs $\langle k \rangle$ approach limit curves for both $\sigma < 1$ and $\sigma \geq 1$ (see the green dashed lines in Fig. 8, which correspond to $n = 20\,000$ and do not evolve for larger graph sizes).

C. Ratio of consecutive eigenvalue spacings and Shannon entropy

Once we have concluded that the average degree is the scaling parameter of $\langle \bar{V}_x \rangle$, our first conjecture is that $\langle k \rangle$ may also be the scaling parameter of $\langle \bar{r} \rangle$ and $\langle \bar{S} \rangle$.

First we normalize $\langle r \rangle$ and $\langle S \rangle$, so that we can compare them for different graph sizes n . We naturally choose $\langle \bar{S} \rangle = \langle S \rangle / \langle S \rangle_{\text{GOE}}$ with $\langle S \rangle_{\text{GOE}} \approx \ln(n/2.07)$ [35]; however, the small-size effects observed for $\langle r \rangle$ and the fact that $\langle r \rangle \rightarrow \text{const} \neq 0$ when $\ell \rightarrow 0$ make us conveniently define $\langle \bar{r} \rangle$ as

$$\langle \bar{r} \rangle = \frac{\langle r \rangle - \langle r(\ell = 0) \rangle}{\langle r(\ell = 2) \rangle - \langle r(\ell = 0) \rangle},$$

where $\langle r(\ell = 0) \rangle$ and $\langle r(\ell = 2) \rangle$, which do not depend on σ , are numerically computed for a given n . Evidently, $\langle r(\ell = 0) \rangle \rightarrow \langle r \rangle_{\text{PE}} \approx 0.3863$ [24] and $\langle r(\ell = 2) \rangle \rightarrow \langle r \rangle_{\text{GOE}} \approx 0.5359$ [24] for large enough n .

Then, in Fig. 9 we present $\langle \bar{r} \rangle$ and $\langle \bar{S} \rangle$ as a function of $\langle k \rangle$; note that the data shown in Fig. 9 are the same as those of Figs. 2(d)–2(i). Even though from this figure we can clearly see that the curves $\langle \bar{X} \rangle$ vs $\langle k \rangle$ fall one on top of the other in each of the figure panels, there is still a small but measurable dependence of these curves on n . That is, while they keep their functional form, they suffer a displacement on the $\langle k \rangle$ axis by increasing n . Therefore, we conclude that $\langle k \rangle$ is not the

scaling parameter of the spectral or the eigenvector properties of the random graph model. Thus, in order to search for the proper scaling parameter ξ we first establish a quantity to characterize the position of the curves $\langle \bar{X} \rangle$ on the $\langle k \rangle$ axis. Since all curves $\langle \bar{X} \rangle$ vs $\langle k \rangle$ transit from zero (PE regime) to one (GOE regime) when $\langle k \rangle$ increases from small to large values, we choose the value of $\langle k \rangle$ for which $\langle \bar{X} \rangle \approx 0.5$ [see the horizontal dashed lines in Figs. 9(b) and 9(e)]. We label the value of $\langle k \rangle$ at half of the PE-to-GOE transition as k^* .

In the insets of Figs. 9(a) and 9(d) we report k^* vs n as extracted from the intersection of the curves $\langle \bar{r} \rangle$ vs $\langle k \rangle$ and $\langle \bar{S} \rangle$ vs $\langle k \rangle$ with the straight lines $\langle \bar{r} \rangle = 0.5$ and $\langle \bar{S} \rangle = 0.5$, respectively. Indeed, the linear trend of the data sets (in log-log scale) k^* vs n suggests the power-law behavior

$$k^* = Cn^\gamma. \tag{15}$$

As shown in the insets of Figs. 9(a) and 9(d), Eq. (15) provides excellent fittings to the data; see the dashed lines. From the fitted exponents, reported in Table I, we can conclude that $\gamma \approx 0.16$ for both the ratio of consecutive eigenvalue spacings and Shannon entropy, for all values of σ .

Finally, we define the scaling parameter as the ratio between $\langle k \rangle$ and k^* , so we get

$$\xi \equiv \frac{\langle k \rangle}{k^*} \propto \frac{\langle k \rangle}{n^\gamma} = n^{-\gamma} \langle k \rangle. \tag{16}$$

Therefore, by plotting again the curves of $\langle \bar{X} \rangle$ now as a function of ξ we observe that curves for different graph sizes n and nonuniformity strengths σ collapse on top of *universal curves* (see Fig. 10). Also note that each measure X is characterized by a slightly different universal curve. In particular we observe that the PE-to-GOE transition is sharper for $\langle \bar{r} \rangle$, as compared to $\langle \bar{S} \rangle$.

D. Straightforward scaling of V_x , r , and S

Above we performed the scaling analysis of V_x , r , and S separately, first for V_x in Sec. V A and later for r and S in Sec. V C. In both cases we took advantage of the previous knowledge of a heuristic expression for $\langle k \rangle$ [see Eqs. (1) and (7)]. However, in other works we have successfully performed scaling studies of both topological and spectral properties of random graph models without any previous insight about the functional form of the scaling parameter (see, e.g., Refs. [27,29,30,32]). Thus, in this section we perform a straightforward scaling analysis of the three measures V_x , r , and S and show that we obtain equivalent results as those reported in Secs. V A and V C.

Taking as a starting point the observations (i–v) made in Sec. III from Fig. 2, in Fig. 11 we present again the measures $\langle X \rangle$ but now they are conveniently normalized as in Figs. 5 and 9. Note that some of the curves presented in Fig. 11

TABLE I. Values of the exponent γ obtained from the fittings of the curves $k^*(X)$ vs n of the insets in Figs. 9(a) and 9(d) with Eq. (15). The average value of γ is reported in the right-most column.

	$\sigma = 0.001$	$\sigma = 0.002$	$\sigma = 0.004$	$\sigma = 0.01$	$\sigma = 0.02$	$\sigma = 0.04$	$\sigma = 0.1$	$\sigma = 0.2$	$\sigma = 0.4$	$\sigma = 0.8$	$\sigma = 1$	$\sigma = \infty$	$\langle \gamma \rangle$
$k^*(r)$ vs n	0.1739	0.1656	0.1659	0.1691	0.1622	0.1672	0.1693	0.1565	0.1461	0.1376	0.1307	0.1297	0.1561
$k^*(S)$ vs n	0.1626	0.1619	0.1614	0.1614	0.1624	0.1613	0.1621	0.1619	0.1509	0.1508	0.1443	0.1455	0.1572

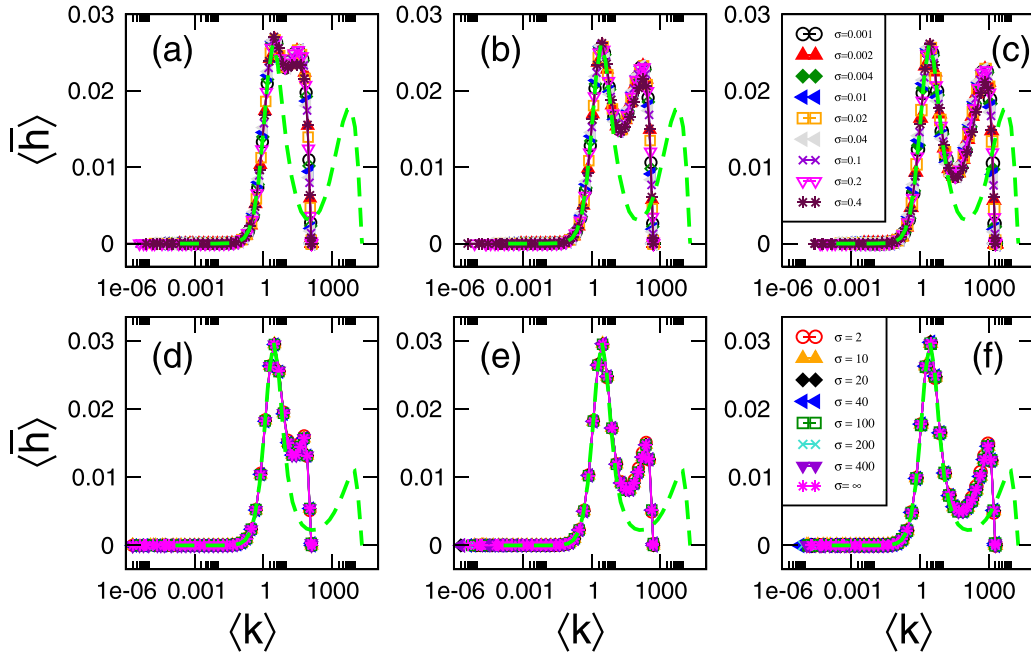


FIG. 8. Average heterogeneity index $\langle \bar{h} \rangle$ normalized to n for [(a), (d)] $n = 125$, [(b), (e)] $n = 500$, and [(c), (f)] $n = 2000$ as a function of the average degree $\langle k \rangle$ of nonuniform RGGs with [(a)–(c)] $\sigma < 1$ and [(d)–(f)] $\sigma \geq 1$. The green dashed lines in [(a)–(c)] [(d)–(f)] correspond to $n = 20000$ and $\sigma = 0.4$ [$n = 20000$ and $\sigma = 10$]. Each data value was computed by averaging over $10^7/n$ random graphs.

were already reported in Fig. 2; however, we are including curves corresponding to additional parameter combinations. From this figure we can clearly see that when changing n and σ the curves $\langle \bar{X} \rangle$ keep their functional form but they suffer a displacement on the ℓ axis. Therefore, in order to search

for the scaling parameter $\chi \equiv \chi(n, \sigma, \ell)$ we first establish a quantity to characterize the position of the curves $\langle \bar{X} \rangle$ on the ℓ axis. Since all curves $\langle \bar{X} \rangle$ vs ℓ transit from zero (PE regime) to one (GOE regime) when ℓ increases from zero to two, we choose the value of ℓ for which $\langle \bar{X} \rangle \approx 0.5$ (see the horizontal

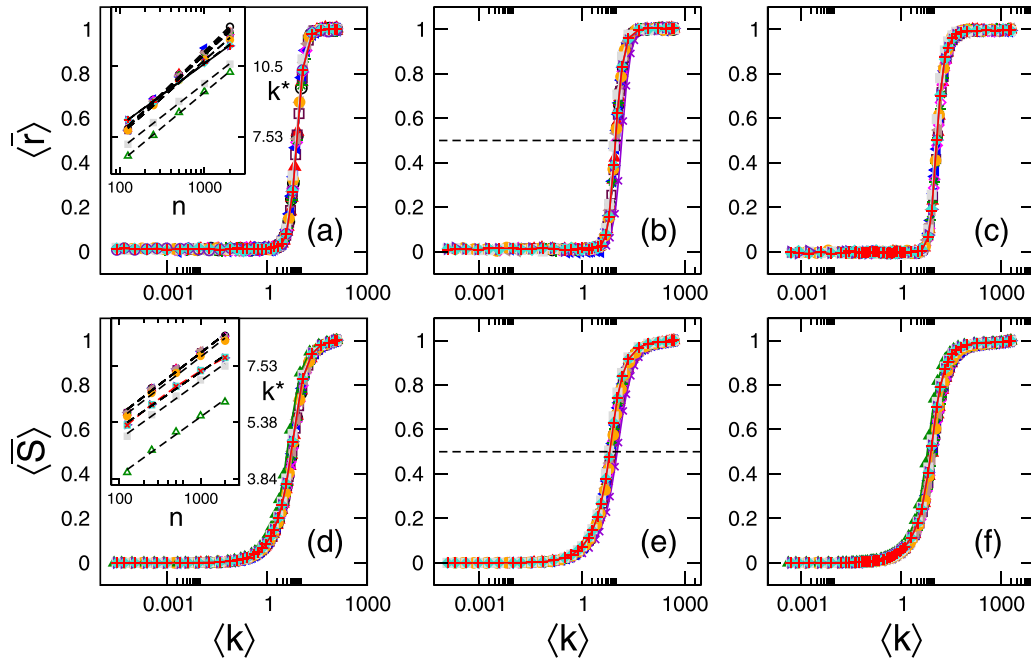


FIG. 9. Normalized [(a)–(c)] average ratio of consecutive eigenvalue spacings $\langle \bar{r} \rangle$ and [(d)–(f)] average Shannon entropy $\langle \bar{S} \rangle$ as a function of the average degree $\langle k \rangle$ of nonuniform RGGs of size [(a), (d)] $n = 125$, [(b), (e)] $n = 500$, and [(c), (f)] $n = 2000$. Same data as in Figs. 2(d)–2(i). The insets in panels (a) and (d) show k^* vs n as extracted from the intersection of the curves $\langle \bar{r} \rangle$ vs $\langle k \rangle$ and $\langle \bar{S} \rangle$ vs $\langle k \rangle$ with the straight lines $\langle \bar{r} \rangle = 0.5$ and $\langle \bar{S} \rangle = 0.5$, respectively. Dashed lines are fittings of the data with Eq. (15). The exponents γ obtained from the fittings are reported in Table I. Horizontal dashed lines in panels (b) and (e) mark $\langle \bar{X} \rangle = 0.5$.

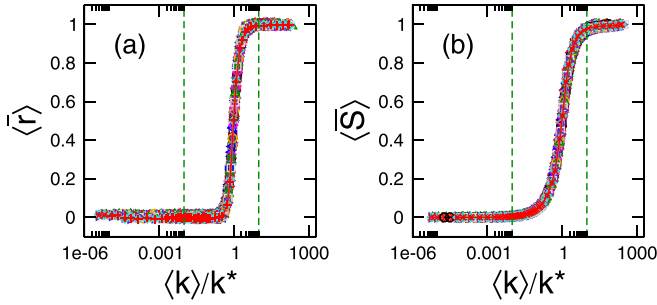


FIG. 10. (a) $\langle \bar{r} \rangle$ and (b) $\langle \bar{S} \rangle$ as a function of the scaling parameter $\xi = \langle k \rangle / k^*$. Same data as in Fig. 9. Vertical dashed lines at $\xi = 0.01$ and 10 mark, approximately, the onset of delocalization and the onset of the GOE regime, respectively.

dashed lines in Fig. 11). We label the value of ℓ at half of the PE-to-GOE transition as ℓ^* , so we call ℓ^* the PE-to-GOE transition point.

Given that ℓ^* depends on both n and σ , in Fig. 12 we report ℓ^* versus n for fixed values of σ (upper panels) and ℓ^* versus σ for fixed values of n (lower panels). It is interesting to notice that while ℓ^* decreases as a function of n (see the upper panels of Fig. 12) for all the values of σ reported here, the curves ℓ^* vs σ show two different behaviors (see the lower panels of Fig. 12): for $\sigma < 1$, ℓ^* grows with σ , but when $\sigma > 1$, $\ell^* \approx \text{const}$, with a transition region around $\sigma_c \approx 1$. Therefore, we define two scaling regimes: the *clustering regime* when $\sigma < \sigma_c$ and the *uniform regime* when $\sigma > \sigma_c$. Note that since σ is given in units of the disk radius, σ_c can be indeed interpreted as the disk radius. These two regimes are exemplified graphically in Fig. 1. In fact, once $\sigma > \sigma_c$ the random graph model proposed here already reproduces the random geometric graph model on the disk. Moreover, the full horizontal lines on top of the data of Figs. 12(d)–12(f) for $\sigma > \sigma_c$ correspond to the value of ℓ^* at $\sigma \rightarrow \infty$; that is, once $\sigma > \sigma_c$, the properties of our random graph model do not change anymore by further increasing σ , as already noticed in Fig. 2.

Indeed, the linear trend of the data sets (in log-log scale) ℓ^* vs n and ℓ^* vs σ suggests the power-law behaviors

$$\ell^* = C n^{-\gamma_\ell} \sigma^\delta. \quad (17)$$

As shown in Fig. 12, Eq. (17) provides excellent fittings to the data; see the dashed lines. From the fitted exponents, reported in Tables II and III, we can safely state that $\gamma_\ell \approx 1/2$ for the number of nonisolated vertices, while $\gamma_\ell \approx 0.43$ for both the ratio of consecutive eigenvalue spacings and Shannon entropy, for all values of σ . Also, $\delta \approx 1/2$ for $\sigma < \sigma_c$ while $\delta \approx 0$ for $\sigma > \sigma_c$, for all the three measures (V_x , r , and S).

TABLE II. Values of the exponent γ_ℓ obtained from the fittings of the curves $\ell^*(X)$ vs n of Figs. 12(a)–12(c) with Eq. (17). The average value of γ_ℓ is reported in the right-most column.

	$\sigma = 0.001$	$\sigma = 0.002$	$\sigma = 0.004$	$\sigma = 0.01$	$\sigma = 0.02$	$\sigma = 0.04$	$\sigma = 0.1$	$\sigma = 0.2$	$\sigma = 0.4$	$\langle \gamma_\ell \rangle$
$\ell^*(V_x)$ vs n	0.5010	0.5015	0.5007	0.5008	0.5013	0.5008	0.5012	0.5012	0.5007	0.5010
$\ell^*(r)$ vs n	0.4316	0.4355	0.4353	0.4333	0.4369	0.4350	0.4343	0.4364	0.4375	0.4350
$\ell^*(S)$ vs n	0.4364	0.4345	0.4348	0.4344	0.4340	0.4346	0.4342	0.4336	0.4331	0.4344

TABLE III. Values of the exponent δ obtained from the fittings of the curves $\ell^*(X)$ vs σ (for $\sigma < 1$) of Figs. 12(d)–12(f) with Eq. (17). The average value of δ is reported in the right-most column.

	$n = 125$	$n = 250$	$n = 500$	$n = 1000$	$n = 2000$	$\langle \delta \rangle$
$\ell^*(V_x)$ vs σ	0.4987	0.4989	0.4983	0.4991	0.4987	0.4987
$\ell^*(r)$ vs σ	0.5013	0.5016	0.5007	0.4994	0.4993	0.5005
$\ell^*(S)$ vs σ	0.5018	0.5007	0.4996	0.5012	0.5025	0.5011

Finally, we define the scaling parameter χ as the ratio between ℓ and ℓ^* , so we get

$$\chi \equiv \frac{\ell}{\ell^*} \propto \frac{\ell}{n^{-\gamma_\ell} \sigma^\delta} = n^{\gamma_\ell} \sigma^{-\delta} \ell. \quad (18)$$

Therefore, by plotting again the curves of $\langle \bar{X} \rangle$ now as a function of χ we observe that curves for different graph sizes n and nonuniformity strengths σ collapse on top of *universal curves* (see Fig. 13).

It is fair to mention that the scaling we found for $\langle \bar{S} \rangle$ when $\sigma > \sigma_c$ is very close to that reported in Ref. [30] for RGGs in the unit square, as expected. There, $\chi \equiv \chi(n, \ell) \propto n^{\gamma_\ell} \ell$ with $\gamma_\ell \approx 0.425$.

At first sight, it seems that in this section we got different scaling parameters than in the previous one: On the one hand, recall that in Sec. V C we found $\xi = \langle k \rangle \propto n \sigma^{-1} \ell^2$ for $\langle \bar{V}_x \rangle$, while we got $\xi = n^{-0.16} \langle k \rangle \propto n^{0.84} \sigma^{-1} \ell^2$ for $\langle \bar{r} \rangle$ and $\langle \bar{S} \rangle$ (here we are using $\langle k \rangle \propto n \sigma^{-1} \ell^2$ when $L \ll 1$ and $\sigma < \sigma_c$). On the other hand, in this section we have obtained $\chi \propto n^{1/2} \sigma^{-1/2} \ell$ for $\langle \bar{V}_x \rangle$ and $\chi \propto n^{0.43} \sigma^{-1/2} \ell$ for $\langle \bar{r} \rangle$ and $\langle \bar{S} \rangle$. This apparent mismatch can be understood by noticing that not only ξ but any function of it should scale the normalized measures $\langle \bar{X} \rangle$; thus, since $\chi \propto \xi^{1/2}$, for the three measures, our results are consistent.

VI. DISCUSSION AND CONCLUSIONS

We performed a detailed scaling study of random geometric graphs (RRGs) in the unit disk characterized by a nonuniform density of vertices. This random graph model may serve as a reference model of complex systems embedded in the plane whose components are not uniformly allocated. The random graph model depends on three parameters: the number of vertices, n ; the degree of nonuniformity, $\sigma \in (0, \infty)$; and the connection radius $\ell \in [0, 2]$. This model produces a cluster around the disk center for $\sigma < \sigma_c$ and reproduces the uniform RGG model in the disk when $\sigma \geq \sigma_c$ (see Fig. 1 and Sec. V D) with $\sigma_c \approx 1$.

By the use of the average degree $\langle k \rangle$, the number of nonisolated vertices, V_x , the ratio of consecutive eigenvalue

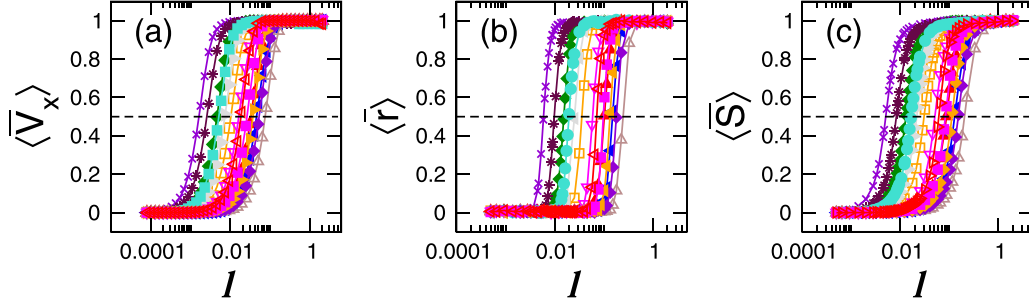


FIG. 11. Normalized (a) number of nonisolated vertices $\langle V_x \rangle$, (b) average ratio of consecutive eigenvalue spacings $\langle \bar{r} \rangle$, and (c) average Shannon entropy $\langle S \rangle$ as a function of the connection radius ℓ of nonuniform RGGs. Each panel displays 14 curves corresponding to the following combinations of (σ, n) : $\{(0.002, 1000), (0.01, 2000), (0.004, 250), (0.04, 2000), (0.02, 500), (0.04, 500), (0.2, 1000), (0.8, 2000), (0.8, 1000), (0.1, 125), (0.8, 500), (0.4, 250), (0.8, 250), (0.8, 125)\}$, from left to right. The dashed lines at $\langle X \rangle = 0.5$ are used to extract ℓ^* ; see the text. Each data value was computed by averaging over $10^7/n$ random graphs.

spacings, r , and the Shannon entropy S of eigenvectors we probe topological as well as spectral properties of our random graph model. First we propose a heuristic expression able to properly describe $\langle k(n, \sigma, \ell) \rangle$ [see Eqs. (1) and (7)]. Then, we looked for the scaling properties of the properly normalized average measure $\langle X \rangle$ (where X stands for V_x , r , and S). As a result of the scaling analysis, we were able to define the scaling parameter, that we label ξ , such that the curves $\langle X \rangle$ vs ξ are invariant curves. Particularly, in the two graph regimes

separated by the nonuniformity σ_c , we found that $\xi = \langle k \rangle$ for $\langle V_x \rangle$ while $\xi = n^{-\gamma} \langle k \rangle$, with $\gamma \approx 0.16$, for $\langle \bar{r} \rangle$ and $\langle S \rangle$. In addition, we found that $\langle V_x \rangle = \langle V_x \rangle/n$ is related to $\langle k \rangle$ as $\langle V_x \rangle \approx 1 - \exp(-\langle k \rangle)$ [see Eq. (9) and Fig. 5].

We stress that the scalings shown in Figs. 5 and 10 have two important consequences in the characterization of the nonuniform random graph model. First, they allow us to define regimes: The PE (GOE) regime can be defined for $\xi < 0.01$ ($\xi > 10$), while $0.01 < \xi < 10$ defines the

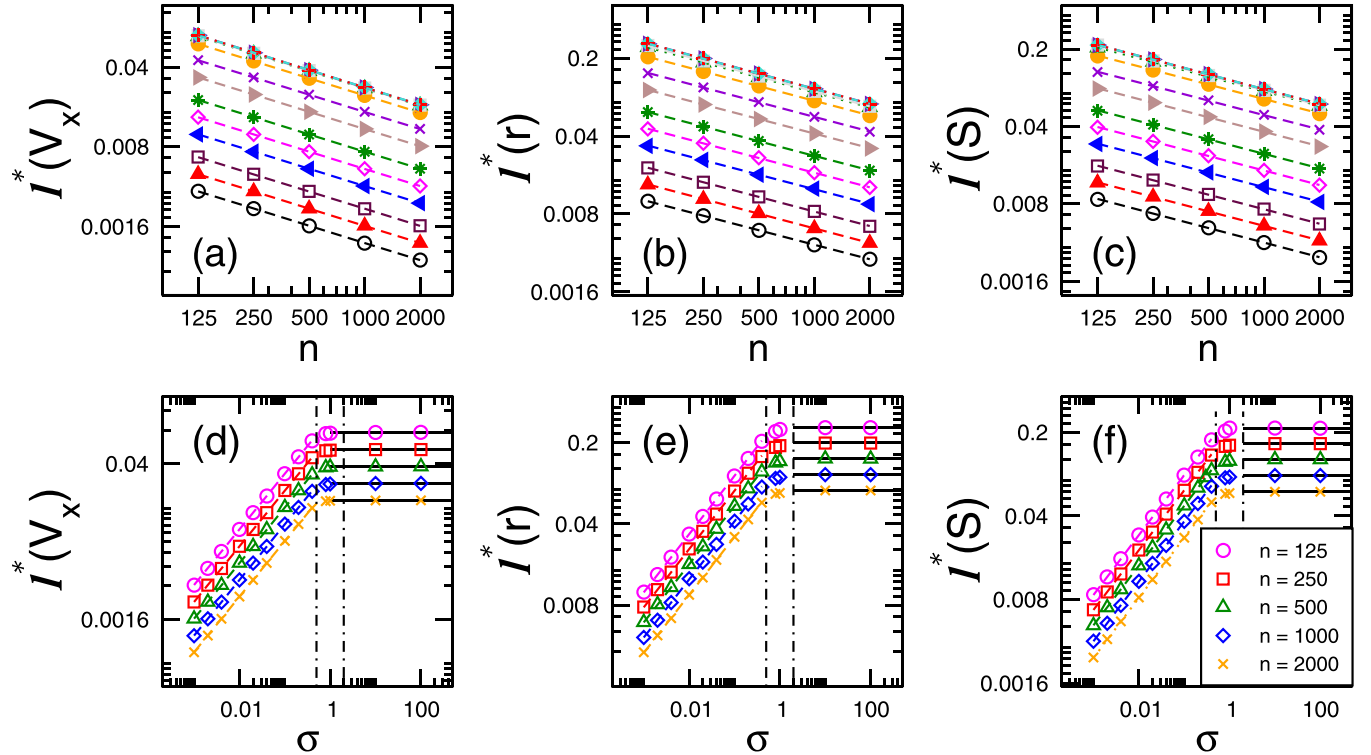


FIG. 12. PE-to-GOE transition point ℓ^* as a function of [(a)–(c)] the graph size n and [(d)–(f)] the nonuniformity σ from [(a), (d)] the number of nonisolated vertices, [(b), (e)] the ratio of consecutive eigenvalue spacings, and [(c), (f)] the Shannon entropy. Several values of σ (n) are reported in the upper (lower) panels. Each of the upper panels [(a)–(c)] displays 14 data sets corresponding to different degrees of nonuniformity σ : $\{0.001, 0.002, 0.004, 0.01, 0.02, 0.04, 0.1, 0.2, 0.4, 0.8, 1, 10, 100, \infty\}$, from bottom to top. The dashed lines are fittings to the data with Eq. (17); the fitted exponents γ_c and δ are reported in Tables II and III, respectively. Dash-dotted vertical lines in the lower panels indicate a transition region around $\sigma_c \approx 1$. Solid lines in the lower panels on top of the data for $\sigma > 1$ correspond to the value of ℓ^* at $\sigma \rightarrow \infty$.

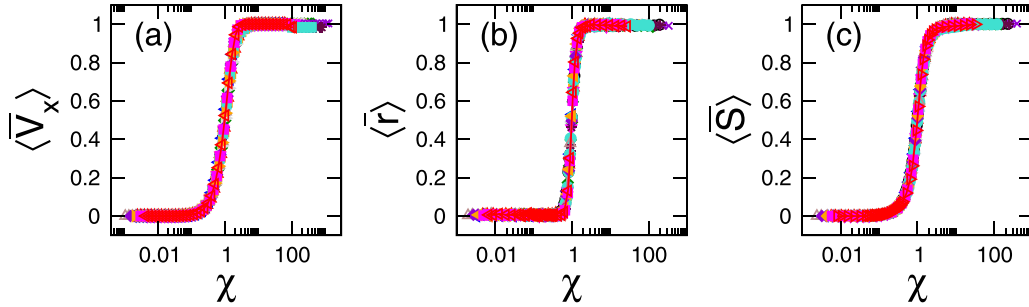


FIG. 13. Normalized (a) number of nonisolated vertices $\langle \bar{V}_x \rangle$, (b) average ratio of consecutive eigenvalue spacings $\langle \bar{r} \rangle$, and (c) average Shannon entropy $\langle \bar{S} \rangle$ as a function of the scaling parameter χ [see Eq. (18)] of nonuniform RGGs. Same curves as in Fig. 11.

PE-to-GOE transition regime. Here, the PE regime is characterized by mostly disconnected vertices and localized eigenvectors while the GOE regime corresponds to almost complete graphs and delocalized eigenvectors. Thus, $\xi = 0.01$ and $\xi = 10$ (see the vertical dashed lines in Figs. 5 and 10) mark, approximately, the percolation transition, or the onset of eigenvector delocalization, and the onset of the GOE limit, respectively. Second, it allow us to make predictions: Given a combination of parameters (n, σ, ℓ) , if $\xi < 0.01$ we know that $\langle V_x \rangle \approx 0$, $\langle r \rangle \approx 0.3863$, and $\langle S \rangle \approx 0$, while if $\xi > 10$ we expect $\langle V_x \rangle \approx n$, $\langle r \rangle \approx 0.5359$, and $\langle S \rangle \approx \ln(n/2.07)$.

It is important to add that the scaling study of spectral and eigenvector properties of nonuniform RGGs shown in Secs. V C and V D could also be done with standard binary adjacency matrices. Indeed, we should arrive at equivalent conclusions. However, when using binary matrices one has to be careful to properly handle the highly degenerate spectra in the limits $\ell \rightarrow 0$ and $\ell \rightarrow 2$, or simply avoid those limits.

We also want to note that the number of nonisolated vertices as well as the Randić connectivity index (see Sec. V B) have provided us with equivalent information as standard RMT measures; that is, we were able to clearly identify both the PE and the GOE regimes, as well as the PE-to-GOE transition regime, by means of the *universal* curves of $\langle \bar{V}_x \rangle$ and $\langle \bar{R} \rangle$ vs ξ . Thus we give further evidence of the usefulness of topological indices in the statistical characterization of random graphs. In addition, we found that $\langle \bar{V}_x \rangle$ is highly correlated with $\langle \bar{S} \rangle$, with a Pearson correlation coefficient approximately

equal to one (as for standard RGGs [25]); therefore, we can guarantee that the randomly weighted adjacency matrix of Eq. (6) indeed describes the corresponding graph model.

Finally, it is relevant to add that once the scaling parameter of the quantities studied here was defined, it is expected that other properties related to the same quantities could also be scaled by the same scaling parameter. As an example, we validate the universality of the scaling parameter ξ by applying it to $\rho(r)$, the probability distribution function of r . In Fig. 14 we present histograms of the probability distribution function of r , $\rho(r)$. Each panel displays six histograms for different combinations of σ and n , while ℓ is tuned in order to produce the same value of ξ . Since the six histograms in each panel fall one on top of the other we can safely say that $\rho(r)$ is invariant for fixed ξ . In addition, we also include in each panel of Fig. 14 the corresponding predictions for $\rho(r)$ for the PE and the GOE [24]:

$$\rho_{\text{PE}}(r) = \frac{2}{(1+r)^2} \tag{19}$$

and

$$\rho_{\text{GOE}}(r) = \frac{27}{4} \frac{r(1+r)}{(1+r+r^2)^{5/2}}, \tag{20}$$

respectively. Note that there is a perfect agreement of $\rho(r)$ with $\rho_{\text{PE}}(r)$ and $\rho_{\text{GOE}}(r)$ when $\xi = 0.1$ and $\xi = 3$, respectively. As expected, for $\xi = 1$, i.e., in the PE-to-GOE transition regime, we observe that the shape of $\rho(r)$ is in between the PE and the GOE predictions.

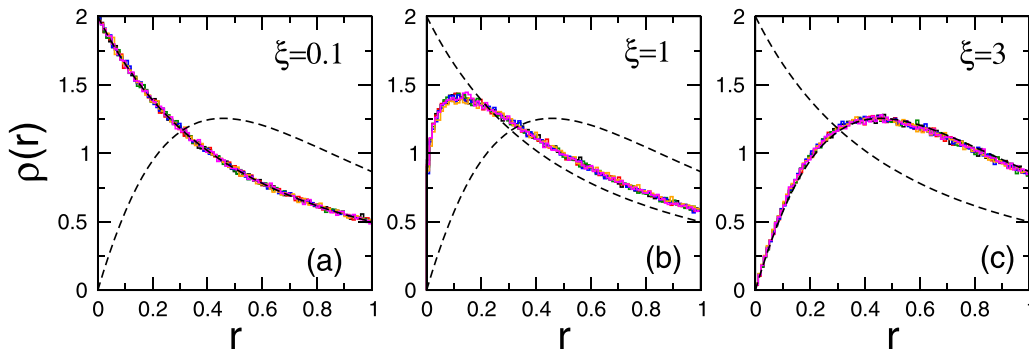


FIG. 14. Histograms of the probability distribution function of the ratio of consecutive eigenvalue spacings $\rho(r)$ for three values of the scaling parameter ξ . Each panel displays six histograms corresponding to the following combinations of (σ, n) : $\{(0.2, 125), (0.04, 250), (0.1, 500), (0.001, 800), (0.02, 1000), (0.01, 2000)\}$. Each histogram was computed from 10^6 ratios. Dashed lines correspond to $\rho_{\text{PE}}(r)$ and $\rho_{\text{GOE}}(r)$ [see Eqs. (19) and (20)].

We hope that this work may motivate further analytical as well as numerical studies on nonuniform random network models and their applications to real-world systems.

ACKNOWLEDGMENTS

J.A.M.-B. acknowledges financial support from CONACyT (Grant No. A1-S-22706) and BUAP (Grant

No. 100405811-VIEP2021). E.E. thanks financial support from Ministerio de Ciencia, Innovación y Universidades, Spain, for Grant No. PID2019-107603GB-I00, “Hubs-repelling/attracting Laplacian operators and related dynamics on graphs/networks.” F.A.R. acknowledges CNPq (Grant No. 309266/2019-0) and FAPESP (Grant No. 19/23293-0) for the financial support given for this research.

-
- [1] M. Barthélémy, Spatial networks, *Phys. Rep.* **499**, 1 (2011).
- [2] E. Estrada, *The Structure of Complex Networks: Theory and Applications* (Oxford University Press, New York, 2011).
- [3] D. Urban and T. Keitt, Landscape connectivity: A graph-theoretic perspective, *Ecology* **82**, 1205 (2001).
- [4] A. Perna, S. Valverde, J. Gautrais, C. Jost, R. Solé, P. Kuntz, and G. Theraulaz, Topological efficiency in three-dimensional gallery networks of termite nests, *Physica A* **387**, 6235 (2008).
- [5] J. Buhl, J. Gautrais, R. V. Solé, P. Kuntz, S. Valverde, J. L. Deneubourg, and G. Theraulaz, Efficiency and robustness in ant networks of galleries, *Eur. Phys. J. B* **42**, 123 (2004).
- [6] E. Santiago, J. X. Velasco-Hernández, and M. Romero-Salcedo, A methodology for the characterization of flow conductivity through the identification of communities in samples of fractured rocks, *Expert Syst. Appl.* **41**, 811 (2014).
- [7] P. Gupta and P. R. Kumar, Critical Power for asymptotic connectivity in wireless networks, in *Stochastic Analysis, Control, Optimization and Applications* (Birkhäuser, Boston, 1999).
- [8] G. J. Pottie and W. J. Kaiser, Wireless integrated network sensors, *Commun. ACM* **43**, 51 (2000).
- [9] D. Estrin, R. Govindan, J. Heidemann, and S. Kumar, Next century challenges: Scalable coordination in sensor networks, in *Proceedings of the ACM/IEEE International Conference on Mobile Computing and Networking* (Scientific Research Publishing, Wuhan, 1999), pp. 263–270.
- [10] E. N. Gilbert, Random graphs, *Ann. Math. Stat.* **30**, 1141 (1959).
- [11] M. Penrose, *Random Geometric Graphs* (Oxford University Press, New York, 2003).
- [12] J. Dall and M. Christensen, Random geometric graphs, *Phys. Rev. E* **66**, 016121 (2002).
- [13] P. Wang and M. C. González, Understanding spatial connectivity of individuals with non-uniform population density, *Philos. Trans. R. Soc. A* **367**, 3321 (2009).
- [14] A. Díaz-Guilera, J. Gómez-Gardeñes, Y. Moreno, and M. Nekovee, Synchronization of Kuramoto oscillators in random geometric graphs, *Int. J. Bif. Chaos* **19**, 687 (2009).
- [15] M. Nekovee, Worm epidemics in wireless ad hoc networks, *New J. Phys.* **9**, 189 (2007).
- [16] V. Isham, J. Kaczmarska, and M. Nekovee, Spread of information and infection on finite random networks, *Phys. Rev. E* **83**, 046128 (2011).
- [17] Z. Toroczkai and H. Guclu, Proximity networks and epidemics, *Physica A* **378**, 68 (2007).
- [18] E. Estrada and M. Sheerin, Random rectangular graphs, *Phys. Rev. E* **91**, 042805 (2015).
- [19] E. Estrada, S. Meloni, M. Sheerin, and Y. Moreno, Epidemic spreading in random rectangular networks, *Phys. Rev. E* **94**, 052316 (2016).
- [20] E. Estrada and G. Chen, Synchronizability of random rectangular graphs, *Chaos* **25**, 083107 (2015).
- [21] E. Estrada and M. Sheerin, Random neighborhood graphs as models of fracture networks on rocks: Structural and dynamical analysis, *Appl. Math. Comput.* **314**, 360 (2017).
- [22] M. Haenggi, J. G. Andrews, F. Baccelli, O. Dousse, and M. Franceschetti, Stochastic geometry and random graphs for the analysis and design of wireless networks, *IEEE J. Sel. Areas Commun.* **27**, 1029 (2009).
- [23] J. Diaz, D. Mitsche, and X. Perez, Dynamic random geometric graphs, [arXiv:cs/0702074](https://arxiv.org/abs/cs/0702074).
- [24] Y. Y. Atas, E. Bogomolny, O. Giraud, and G. Roux, Distribution of the Ratio of Consecutive Level Spacings in Random Matrix Ensembles, *Phys. Rev. Lett.* **110**, 084101 (2013).
- [25] R. Aguilar-Sanchez, J. A. Mendez-Bermudez, F. A. Rodrigues, and J. M. Sigarreta-Almira, Topological versus spectral properties of random geometric graphs, *Phys. Rev. E* **102**, 042306 (2020).
- [26] G. Torres-Vargas, R. Fossion, and J. A. Mendez-Bermudez, Normal mode analysis of spectra of random networks, *Physica A* **545**, 123298 (2020).
- [27] C. T. Martínez-Martínez, J. A. Mendez-Bermudez, Y. Moreno, J. J. Pineda-Pineda, and J. M. Sigarreta, Spectral and localization properties of random bipartite graphs, *Chaos Soliton Fract.* **X 3**, 100021 (2019).
- [28] T. Peron, B. M. F. de Resende, F. A. Rodrigues, L. da F. Costa, and J. A. Mendez-Bermudez, Spacing ratio characterization of the spectra of directed random networks, *Phys. Rev. E* **102**, 062305 (2020).
- [29] J. A. Mendez-Bermudez, A. Alcazar-Lopez, A. J. Martínez-Mendoza, F. A. Rodrigues, and T. K. DM. Peron, Universality in the spectral and eigenfunction properties of random networks, *Phys. Rev. E* **91**, 032122 (2015).
- [30] L. Alonso, J. A. Mendez-Bermudez, A. Gonzalez-Melendrez, and Y. Moreno, Weighted random-geometric and random-rectangular graphs: Spectral and eigenfunction properties of the adjacency matrix, *J. Complex Networks* **6**, 753 (2018).
- [31] L. Alonso, J. A. Mendez-Bermudez, and E. Estrada, Geometrical and spectral study of β -skeleton graphs, *Phys. Rev. E* **100**, 062309 (2019).
- [32] J. A. Mendez-Bermudez, G. Ferraz-de-Arruda, F. A. Rodrigues, and Y. Moreno, Scaling properties of multilayer random networks, *Phys. Rev. E* **96**, 012307 (2017).
- [33] *The Oxford Handbook of Random Matrix Theory*, edited by G. Akemann, J. Baik, and P. DiFrancesco (Oxford University Press, Oxford, 2015).

- [34] A. D. Jackson, C. Mejia-Monasterio, T. Rupp, M. Saltzer, and T. Wilke, Spectral ergodicity and normal modes in ensembles of sparse matrices, *Nucl. Phys. A* **687**, 405 (2001).
- [35] B. Mirbach and H. J. Korsh, A generalized entropy measuring quantum localization, *Ann. Phys. (NY)* **265**, 80 (1998).
- [36] R. Aguilar-Sanchez, I. F. Herrera-Gonzalez, J. A. Mendez-Bermudez, and J. M. Sigarreta, Computational properties of general indices on random networks, *Symmetry* **12**, 1341 (2020).
- [37] M. Randić, On characterization of molecular branching, *J. Am. Chem. Soc.* **97**, 6609 (1975).
- [38] *Recent Results in the Theory of Randić Index*, edited by I. Gutman and B. Furtula (University of Kragujevac, Kragujevac, 2008).
- [39] X. Li and I. Gutman, *Mathematical Aspects of Randić Type Molecular Structure Descriptors* (University of Kragujevac, Kragujevac, 2006).
- [40] X. Li and Y. Shi, A survey on the Randić index, *MATCH Commun. Math. Comput. Chem.* **59**, 127 (2008).
- [41] I. Gutman, B. Furtula, and V. Katanić, Randić index and information, *AKCE Int. J. Graphs Comb.* **15**, 307 (2018).
- [42] N. Nikolova and J. Jaworska, Approaches to measure chemical similarity—a review, *QSAR Comb. Sci.* **22**, 1006 (2003).
- [43] M. Randić, On the history of the connectivity index: From the connectivity index to the exact solution of the protein alignment problem, *SAR QSAR Environ. Res.* **26**, 1 (2015).
- [44] E. Estrada, Quantifying network heterogeneity, *Phys. Rev. E* **82**, 066102 (2010).
- [45] P. de Meo, F. Messina, D. Rosaci, G. M. L. Sarné, and A. V. Vasilakos, Estimating graph robustness through the Randić index, *IEEE Trans. Cybern.* **48**, 3232 (2018).
- [46] C. T. Martinez-Martinez, J. A. Mendez-Bermudez, J. M. Rodriguez, and J. M. Sigarreta-Almira, Computational and analytical studies of the Randić index in Erdős-Rényi models, *Appl. Math. Comput.* **377**, 125137 (2020).